

# A STUDY OF TRANSITION REGION AND CORONAL DOPPLER SHIFTS IN A SOLAR CORONAL HOLE

M. D. Popescu<sup>1,2</sup> and J. G. Doyle<sup>1</sup>

<sup>1</sup> Armagh Observatory, College Hill, Armagh BT61 9DG, N. Ireland

<sup>2</sup> Astronomical Institute of the Romanian Academy, RO-75212 Bucharest 28, Romania

## ABSTRACT

We present a study of a high spatial resolution raster scan taken on-disk with the SoHO/SUMER spectrograph in a solar polar Coronal Hole (CH) region. We have analysed the line shifts and widths of two EUV emitting ions, O III 703.87 Å and Mg IX 706.02 Å. Our results confirm plasma outflows from CHs. In particular, the correlation between the intensity and the Doppler velocity in the case of the O III line constitute the lowest precise indication of fast wind streams seen originating from the network boundaries in the transition region.

Key words: Sun: EUV radiation; Doppler line-shifts; coronal holes; chromospheric network; fast solar wind.

## 1. INTRODUCTION

A CH was first identified as source of a high velocity solar wind stream by Krieger et al. (1973), who compared soft X-ray solar data taken during a sounding rocket flight on 24 November 1970 with the wind velocity measured outside the terrestrial atmosphere. Further improvements in the construction of UV spectrographs soon allowed the determination of coronal plasma Doppler velocities. Data taken with a sounding rocket on 30 August 1973 led to the determination of an outflow velocity from the CHs of  $\approx 16 \text{ km s}^{-1}$  in the Si XI 303 Å, Mg IX 368 Å and Mg X 610 Å lines (Cushman & Rense, 1976).

Recently, observations collected with SoHO UV spectrometers have greatly helped in achieving more precise results about properties of plasma from different layers of the solar atmosphere. Due to its high spatial, temporal and especially spectral resolution, the SUMER (Solar Ultraviolet Measurements of Emitted Radiation) grating spectrograph on SoHO (Wilhelm et al., 1995, Wilhelm et al., 1997, Lemaire et al., 1997) is currently the most suitable instrument for plasma velocity diagnostics as inferred from a wide range of EUV lines.

Using on-disk observations from SUMER, signatures of outflows in CHs were deduced by Warren et al. (1997), Dammasch et al. (1999), Hassler et al. (1999), Peter &

Judge (1999), Peter (1999), Stucki et al. (2000a), Stucki et al. (2000b), Wilhelm et al. (2000), Xia et al. (2003) and Popescu & Doyle (2003).

All the mentioned authors agreed about a blue-shift of CH plasma between 3 and 10  $\text{km s}^{-1}$  in lines originating above  $\approx (5 - 6) \times 10^5 \text{ K}$ . At lower temperatures, evidence for outflow of fast solar wind from CHs was found by Peter & Judge (1999) and Popescu & Doyle (2003).

As the spatial resolution of the instrumentation increased, the quest was to find more precisely what are the small-scale features responsible for the development and rise of the fast solar wind streams from CHs. For this purpose, one needs to correlate the plasma up or down motions with the fine structures inside the CHs, which are only seen from the low transition region downward. The difficulty of this study is that both the spectral and the spatial resolution of data needs to be high enough in order to precisely determine the small-scale velocity patterns and the chromospheric CH features.

Hassler et al. (1999) reported correlations between the plasma outflow as deduced from the coronal Ne VIII 770 Å line and the chromospheric network as seen in the Si II 1533 Å line. Stucki et al. (2000b) confirmed these results, by comparing the Ne VIII line-of-sight (LOS) velocity with the N IV 765 Å intensity.

Here, we provide evidence for outflows of CH plasma from the chromospheric network boundaries, by direct comparison of the O III 703 Å Doppler velocity with the intensity of the same low TR ion. This study constitute the first precise indication of fast wind streams seen originating from the CH network boundaries at such a low height in the TR. In the following we explain how the data were processed and interpreted and we give a summary of the results.

## 2. DATA

We analysed a solar on-disk raster scan taken in a northern Pole CH region on 17 March 1999 (K. Wilhelm) with the  $(1 \times 300) \text{ arcsec}^2$  slit of detector B from SUMER. Because the end of each scan was clipped, the final image

dimension is  $(72 \times 230)$  arcsec<sup>2</sup>, with a spatial resolution of  $\approx 1$  arcsec and a spectral resolution of 22.4 mÅ. The raster was taken during 01h 04m – 04h 07m UT, each scan having an integration time of 150 s.

Standard SUMER calibration procedures were applied, as described in Popescu & Doyle (2003).

The collected (1<sup>st</sup> order) spectrum covered an approximate 23 Å spectral region centered around 709 Å. The emission lines of this spectral interval were identified from the SUMER Atlas of Curdt et al. (2001). We studied the shifts and widths of a low TR line, O III 703.87 Å ( $\approx 8 \times 10^4$  K) and a coronal line, Mg IX 706.02 Å ( $\approx 10^6$  K). The approximative formation temperature in ionization equilibrium was taken from Mazzotta et al. (1998).

As the data were taken on-disk, the O III line is strong enough and no additional spatial binning was needed, but the relatively weak intensity of the coronal line did not allow a similarly high spatial resolution analysis. Therefore, for the Mg IX 706 Å line we had to perform a  $(4 \times 4)$  arcsec<sup>2</sup> pixel binning on the spatial *solar x* and *solar y* coordinates.

The final aim of our study was to calculate the intensities and the Doppler velocities (line of sight, or LOS velocities) of both lines considered. With that purpose, we had to determine: the position of the spectrum center in each (*solar x*, *solar y*) coordinate, for calculating the LOS velocity, as well as the amplitude and the full width at half maximum (*FWHM*), for calculating the raster intensity.

The pixel position was found by applying a Gaussian fit (with the XCFIT program from the SoHO data analysis software) to the binned spectrum of all *solar x* and *solar y* pixels, that gave us a good signal-to-noise ratio for the entire CH raster. We converted the pixel to Å by taking O III 703.87 Å as the reference line.

When fitting the central wavelength position for each pixel along the *solar y* slit, there was a linear drift in wavelength with distance along the slit for both O III 703 Å and Mg IX 706 Å lines, which had to be corrected.

Trying to find whether there is a correlation between the Doppler velocity and the intensity for the O III line, we made one dimensional cuts at different pixel positions on the *solar x* axis which we discuss below.

In order to obtain an absolute wavelength calibration, the line position as determined at the limb was assumed to have a zero shift. That made necessary an additional correction of about 1 km s<sup>-1</sup> for the O III 703 Å line and less than 0.5 km s<sup>-1</sup> for the Mg IX 706 Å line.

We also corrected the measured *FWHM* for the contribution of the instrumental profile, using the provided software.

Considering that the Gaussian profile is a good approximation for optically thin lines, we applied a fitting procedure (with the XCFIT BLOCK program from the SoHO

software package). From the determined amplitude, position and width, we calculated the Doppler velocity and the intensity for the O III 703 Å and Mg IX 706 Å lines.

### 3. RESULTS

We finally obtained Doppler velocity and intensity maps of the two considered lines. The spatial resolution of the images is  $(1 \times 1)$  arcsec<sup>2</sup> for the TR line and  $(4 \times 4)$  arcsec<sup>2</sup> for the coronal line.

In the coronal line, the CH is seen as a reduction in the intensity, surrounded by the brighter quiet Sun (QS), and very well correlated with negative Doppler velocities (outflows) of about  $-4$  km s<sup>-1</sup>.

In the O III line, the bright chromospheric network is clearly distinguishable in the intensity plot with the coronal hole showing a quiet Sun pattern. As the spatial resolution of this low TR line is just at the limit of the detector (1 arcsec), both the intensity and the Doppler velocity maps show very fine characteristics which are difficult to be correlated. This is why, in order to see the correlation between the Doppler velocity and the intensity for the O III line, we made one dimensional cuts at different pixel positions on the *solar x* axis.

Looking at one-dimensional plots, the motion of the plasma from different features in the TR is very easily recognizable. In Figure 1 we give as examples two *solar x* positions of the raster in the Mg IX line and six in O III, plotting the intensity and the Doppler velocity along the *solar y* direction. The selected positions are: *solar x* = 8 on the Mg IX  $(4 \times 4)$  arcsec<sup>2</sup> plot, corresponding to *solar x* = 31, 32 and 33 on the O III  $(1 \times 1)$  arcsec<sup>2</sup> plot (left panels) and *solar x* = 15 on the Mg IX plot, corresponding to *solar x* = 59, 60 and 61 on the O III plot (right panels). We have chosen these positions because on the first cut we have the bright coronal point and, as we will show later, on the second selection there is an explosive event. Examples of CH and QS network boundaries can be found at any selection chosen on the *solar x* axis.

The intensity is plotted as a dashed line and the Doppler velocity as a continuous line, with the corresponding  $\approx 2$  km s<sup>-1</sup> error. We have determined the error from the fitting procedure to be no more than 2 km s<sup>-1</sup>; in some instances (depending mostly on the signal-to-noise ratio of the spectra), the errors were even less than 1 km s<sup>-1</sup>.

We have divided the high values of the intensity into four categories. Plasma motion presents different trends in each of those four types of bright features. This is why a statistics of plasma velocities in relation to the values of the intensity can not reveal the full story, as a careful examination of each individual increase in the intensity is needed.

We have selected a few examples of those four type of phenomena as follows (see Figure 1):

- coronal bright point: feature (a);

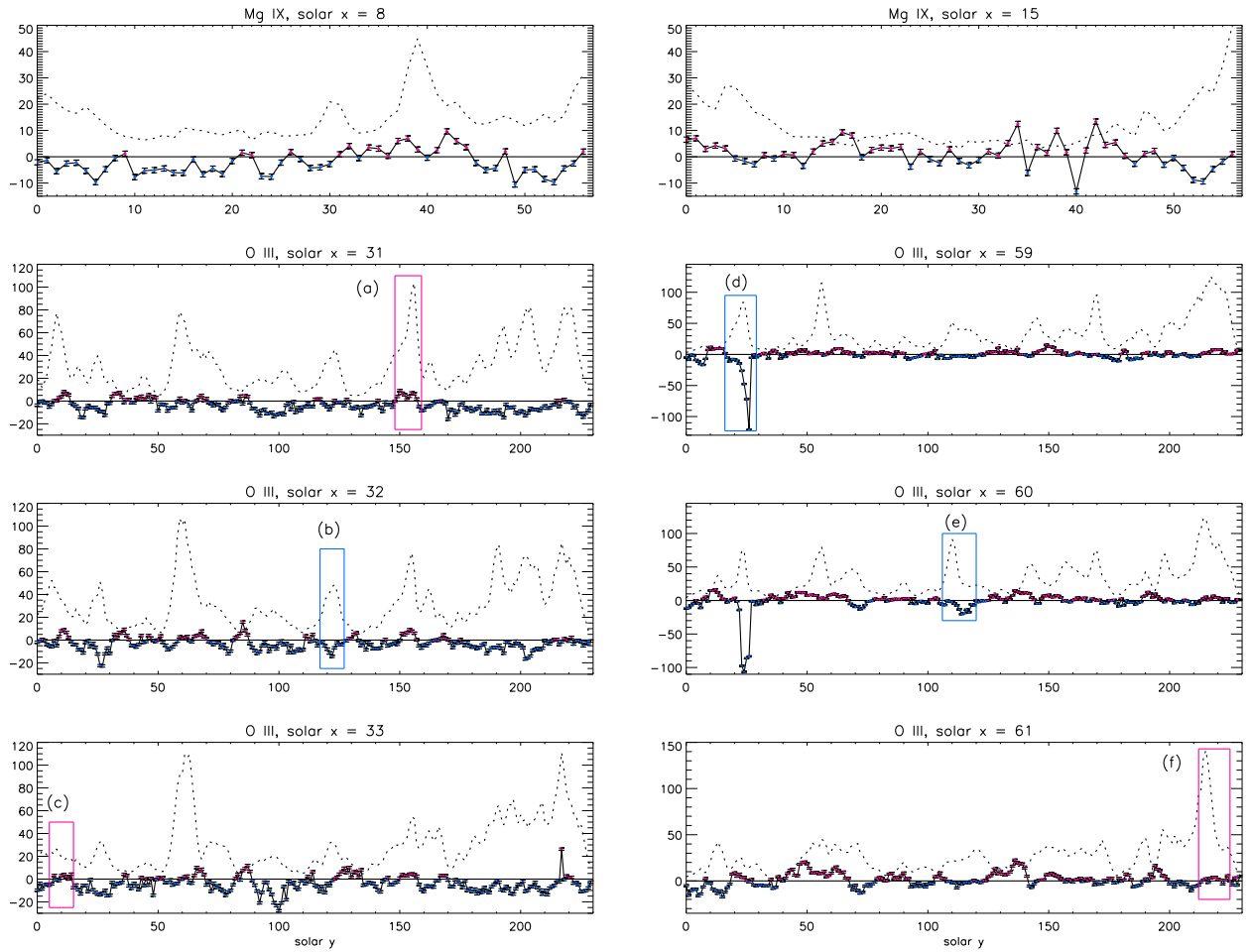


Figure 1. Mg IX  $706 \text{ \AA}$  and O III  $703 \text{ \AA}$  intensity (dotted line) and Doppler velocity plots (solid line with error bars) for the selected regions. The plots represent two sections along the solar y axis for the Mg IX line (on top of the figure), each followed by three corresponding sections for the O III line. The identified features are: (a) coronal BP; (b and e) CH chromospheric network boundaries; (c and f) QS network boundaries and (d) explosive event. The spatial resolution is of 1 arcsec for O III and 4 arcsec for Mg IX.

- CH chromospheric network boundaries: features (b) and (e);
- QS chromospheric network boundaries: features (c) and (f);
- explosive event: feature (d).

The coronal bright point (BP) is seen as an increase in the Mg ix intensity, which corresponds to a high value of the O iii intensity. The chromospheric network is seen as high values in the O iii intensity (that do not correspond to the coronal BP). Differentiating between the bright network inside and outside the CH is very simple, as above the O iii plots we have the coronal Mg ix line in which CH boundaries clearly appear as increases in the intensity. Note that the Mg ix and O iii are spatially aligned, as the 57 units from the Mg ix *solar y* correspond with the 230 units from the O iii plot.

Establishing which of the high values from the O iii intensity represents an EUV explosive event was more challenging, but was done by looking at individual spectra. Large fitting errors indicate a highly dynamic environment. When visualizing each spectrum, for the points in which the fitting error is high, we indeed saw very enhanced wings or even a double Gaussian appearance, where a single Gaussian is evidently not a good fit anymore.

In Figure 2 we plot each spectra for a few *solar y* positions on the selected cuts in the O iii line, at the location of the selected features (a) – (f). The increased line widths at position *solar x* = 59, feature (d), indicate the presence of the explosive event, which is clearly seen despite the time length of the scan ( $\approx 150$  s).

The intensity values in the bright point and in the explosive event are not much higher than many of the values from the network boundaries, meaning that intensity values alone do not help us to distinguish among those four types of features.

A simple visual inspection of the one-dimensional plots, bearing in mind the classification scheme detailed above, reveals that for each of the four types of increases in the intensity, the corresponding Doppler velocity has the tendency to display a certain behaviour.

The BP – feature (a) in Figure 1 – is surrounded by redshifts of around  $5\text{--}10 \text{ km s}^{-1}$  and just in the middle, the velocity decreases toward zero. This very interesting feature is observed in both O iii and Mg ix lines. A similar result for a BP was found by Wilhelm et al. (2000), who reported zero or outward directed LOS velocities in the Ne VIII line, and by Madjarska et al. (2003), who observed more precisely that the BP is dominated by redshifts (up to  $\approx 10 \text{ km s}^{-1}$ ) but in a small area it is blue-shifted. Madjarska et al. (2003) data was a high cadence temporal series acquired with SUMER, in the S vi 933 Å line (originating at an intermediate height between our two lines, corresponding to  $\approx 2 \times 10^5$  K). Moreover, the authors also compared their data with MDI magnetograms, and saw that the blue-shifted region was located between the two magnetic polarities.

Chromospheric network boundaries – features (b) and (e) – are blue-shifted with velocities varying between  $-4$  and  $-10 \text{ km s}^{-1}$  (median value  $\approx -7 \text{ km s}^{-1}$ ). Their average dimension is about  $13 \text{ arcsec} \approx 9000 \text{ km}$ .

Inside the CH, one can see that every time there is a decrease in the intensity, it corresponds to increases in the velocity, which, generally, becomes red-shifted. That would mean that in the dark inter-network cells plasma moves downward, with an average speed of  $\approx 5 \text{ km s}^{-1}$ . The average dimension of the cells is around  $5\text{--}6$  pixels  $\approx 4000 \text{ km}$  on the Sun.

In the QS – features (c) and (f) – the plasma behaviour is completely changed, with O iii intensity increases in the network being red-shifted with  $\approx 5 \text{ km s}^{-1}$ .

In the explosive event – feature (d) – solar plasma undergoes rapid movements. As seen in Figure 3 (d) at *solar x* = 59, the spectrum shows a double peak structure. In this region, the single Gaussian fit is not appropriate, as it obviously gives very high errors. When we fitted the spectra from the explosive event with a double Gaussian, we found outflow velocities up to  $-120 \text{ km s}^{-1}$ .

In Figure 2, the line shifts toward red (to the right) indicate redshifts (downward motion) in the PB and QS network boundaries: features (a), (c) and (f) and toward blue (to the left) indicate blue-shifts (upward motion) in the explosive event and CH network boundaries: features (b), (d) and (e).

We have observed that the dimension of the inter-network cells is generally smaller than that of the bright CH network boundaries. As regards the velocity structures, one can observe that they are smaller than the intensity ones and they also have a tendency to be asymmetric. Similar characteristics were reported by Gontikakis et al. (2003) in their study of TR structures in the QS (Si II 1533 Å C IV 1548 Å and Ne VIII 770 Å lines). They suggest that the larger width of the network boundaries are due to the opening of the magnetic field lines from the convective cells boundaries, when they reach higher levels in the atmosphere, while the smaller velocity structure and asymmetry could be due to the fact that different structures may show different Doppler shifts even if they have comparable intensities, and also to the asymmetric heating that may induce different flows in different locations.

#### 4. CONCLUSIONS

Our results are in agreement with the net CH blue-shifts observed in the TR and low corona, as well as with the red-shifts reported for the QS regions. In the case of the low TR line, the roots of the outflows correspond to the bright, highly structured network boundaries, while for the coronal line the upward LOS velocity is seen in the dark area of the CH.

CH outflows up to  $10 \text{ km s}^{-1}$  were previously reported. Dammasch et al. (1999) reports Ne VIII outflow speeds in CH regions of  $\approx 9 \text{ km s}^{-1}$ . A blue-shift of  $3\text{--}6 \text{ km s}^{-1}$  is reported by Hassler et al. (1999) for the same line. CH

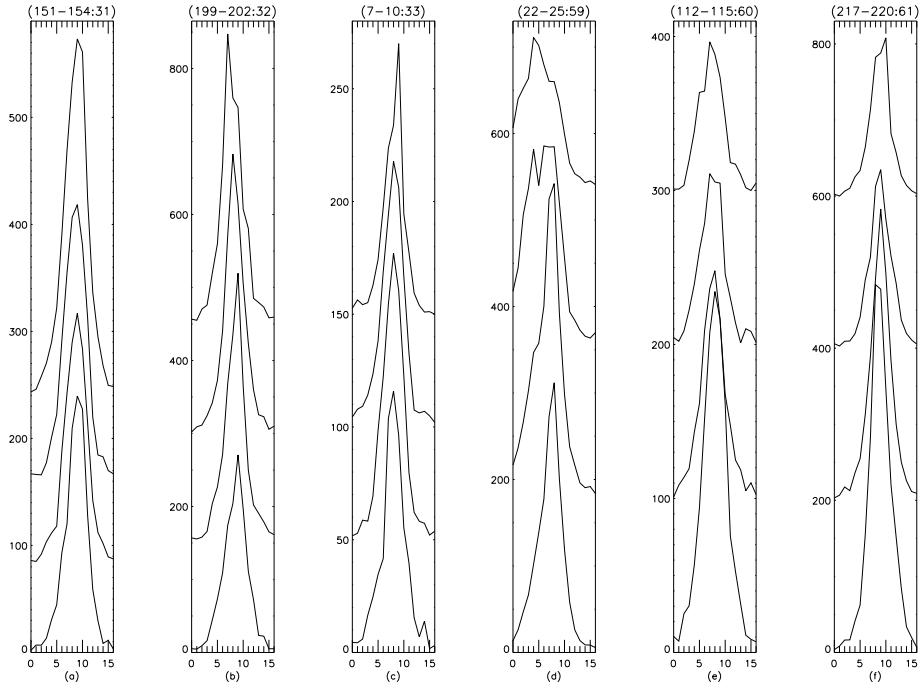


Figure 2. Spectra of the  $O\text{ III}$  line for four positions along the solar  $y$  axis on the selected solar  $x$  cuts. The  $x$  axis is given in spatial pixels. The blue- and red-shifted wings for each increase in the intensity are easy to distinguish. The line shifts toward red (to the right) indicate redshifts (downward motion) in the PB and QS network boundaries – see features (a), (c) and (f) – and toward blue (to the left) indicate blue-shifts (upward motion) in the explosive event and CH network boundaries – features (b), (d) and (e). The increased line widths, together with a double Gaussian shape for solar  $x = 59$  are the signature of an explosive event.

blue-shifts for large samples of TR lines were found by Peter & Judge (1999) and Stucki et al. (2000). The average blue-shift deduced in CHs by Wilhelm et al. (2000) is of  $\approx 3\text{ km s}^{-1}$  for both He I and Ne VIII. The Ne VIII line in an equatorial CH analysed by Xia et al. (2003) is blue-shifted with an average velocity of  $\approx 7.5\text{ km s}^{-1}$ .

In our data, for the Mg IX 706 Å line, the net LOS velocity in the CH is  $\approx -1\text{ km s}^{-1}$  (average over all velocity values from the CH). The blue-shifted material alone in the CH has an average velocity of  $\approx -4\text{ km s}^{-1}$ .

From the characteristics of the radiation emitted by the  $O\text{ III}$  ion, we can define the following: in CH network boundaries, plasma is blue-shifted with an average velocity of  $-7\text{ km s}^{-1}$ ; for the network outside the CH, the corresponding LOS velocity is red-shifted with  $\approx 5\text{ km s}^{-1}$ ; explosive events dislocate plasma to outflow velocities as high as  $-120\text{ km s}^{-1}$ ; the X-ray BP corresponds to a small portion of zero LOS velocities, in the middle of the structure, surrounded by positive (upward) values of about  $5\text{--}10\text{ km s}^{-1}$ .

As reported in Popescu & Doyle 2003, our work provided the first result of plasma motion at such a low atmospheric height (close to the base of the TR,  $\approx 8 \times 10^4\text{ K}$ ) in a CH, at a spatial resolution high enough to distinguish the fine-scale correspondence between the network patterns and the plasma up-flows.

Previous works showed strong evidence in favour of the solar wind outflow as observed in CHs, but none of

them found any correlation between the network intensity and the Doppler velocity of the TR lines. We suppose that is due to the coarse spatial scale in which the TR lines characteristics were determined. The only correlations reported between the plasma outflow and the chromospheric network were of Doppler velocities from the coronal Ne VIII line and intensities from lower temperatures.

Even if Peter & Judge (1999) analysed a large sample of lines over the whole TR, the CH data were taken while SoHO was rolling, so the small-scale spatial structures along the slit were largely smeared out over  $100\text{ arcsec}$ – $200\text{ arcsec}$ . This allowed them to determine the variation of the Doppler shift over a large spatial scale, but the spatial resolution was not sufficient to help them finding any relation between the line width and the intensity.

Hassler et al. (1999) clearly observed the outflow motions in the Ne VIII, but not in the other two ions analysed: C III and Si II, therefore they correlated the Doppler velocity of the Ne VIII ions with the network boundaries inferred from the intensities of Si II. The data were spatially binned over  $(3 \times 3)\text{ arcsec}^2$ . Similarly, Stucki et al. (2000b) compared Ne VIII velocities with intensities from lower TR heights and found the same correlation between those two quantities. Moreover, they show that in the temperature range from  $2 \times 10^4\text{ K}$  to  $2 \times 10^5\text{ K}$  there is a difference between the CH and the QS. Their data were binned over 20 pixels.

Xia et al. (2003) correlated the Ne VIII intensities and

LOS velocities with solar magnetograms, finding that the larger blue-shifts are seen mainly in regions with high concentrations of unipolar magnetic field.

Our results (see also Popescu & Doyle, 2003) constitute the first precise indication of fast wind streams seen originating from the CH network boundaries at such a low height in the TR. We have derived this conclusion from direct correlation between the O III 703 Å Doppler velocity and the intensity of the same ion.

#### ACKNOWLEDGMENTS

This work was supported in part by PPARC grant PPA/G/S/1999/00055 and by the Programme for Research in Irish Third Level Institutions for Grid-enabled Computational Physics of Natural Phenomena (Cosmo-Grid). The SUMER project is financially supported by DLR, CNES, NASA, and PRODEX. Research at Armagh Observatory is grant-aided by the N. Ireland Dept. of Culture, Arts and Leisure.

#### REFERENCES

- Curdt, W., Brekke, P., Feldman, U., Wilhelm, K., Dwivedi, B. N., Schühle, U., & Lemaire, P. 2001, *A & A*, 375, 591
- Cushman, G. W. & Rense, W. A. 1976, *ApJ Lett.*, 207, L61
- Dammasch, I. E., Wilhelm, K., Curdt, W., & Hassler, D. M. 1999, *A & A*, 346, 285
- Gontikakis, C., Peter, H., & Dara, H. C. 2003, *A & A*, 408, 743
- Hassler, D. M., Dammasch, I. E., Lemaire, P., Brekke, P., Curdt, W., Mason, H. E., Vial, J., & Wilhelm, K. 1999, *Science*, 283, 810
- Krieger, A. S., Timothy, A. F., & Roelof, E. C. 1973, *Sol. Phys.*, 29, 505
- Lemaire, P. et al. 1997, *Sol. Phys.*, 170, 105
- Madjarska, M. S., Doyle, J. G., Teriaca, L., & Banerjee, D. 2003, *A & A*, 398, 775
- Mazzotta, P., Mazzitelli, G., Colafrancesco, S., & Vittorio, N. 1998, *A & A Suppl.*, 133, 403
- Peter, H. 1999, *ApJ*, 516, 490
- Peter, H. & Judge, P. G. 1999, *ApJ*, 522, 1148
- Popescu, M. D. & Doyle, J. G. 2003, *A & A*, (submitted)
- Stucki, K., Solanki, S. K., Schühle, U., & Rüedi, I. 2000, *A & A*, 362, L49
- Stucki, K., Solanki, S. K., Schühle, U., Rüedi, I., Wilhelm, K., Stenflo, J. O., Brković, A., & Huber, M. C. E. 2000, *A & A*, 363, 1145
- Warren, H. P., Mariska, J. T., & Wilhelm, K. 1997, *ApJ Lett.*, 490, L187
- Wilhelm, K. et al. 1995, *Sol. Phys.*, 162, 189
- Wilhelm, K. et al. 1997, *Sol. Phys.*, 170, 75
- Wilhelm, K., Dammasch, I. E., Marsch, E., & Hassler, D. M. 2000, *A & A*, 353, 749
- Xia, L. D., Marsch, E., & Curdt, W. 2003, *A & A Lett.*, 399, L5